

# Filling the disk hollow following binary black hole merger: The transient accretion afterglow

Stuart L. Shapiro<sup>1,\*</sup>

<sup>1</sup>*Department of Physics, University of Illinois at Urbana-Champaign, Urbana, IL 61801*

(Dated: March 4, 2022)

Tidal torques from a binary black hole (BHBH) empty out the central regions in any circumbinary gaseous accretion disk. The balance between tidal torques and viscosity maintain the inner edge of the disk at a radius  $r \sim 1.5a - 2a$ , where  $a$  is the binary semimajor axis. Eventually, the inspiraling binary decouples from disk and merges, leaving behind a central hollow (“donut hole”) in the disk orbiting the remnant black hole. We present a simple, time-dependent, Newtonian calculation that follows the secular (viscous) evolution of the disk as it fills up the hollow down to the black hole innermost stable circular orbit and then relaxes to stationary equilibrium. We use our model to calculate the electromagnetic radiation (“afterglow”) spectrum emitted during this transient accretion epoch. Observing the temporal increase in the total electromagnetic flux and the hardening of the spectrum as the donut hole fills may help confirm a BHBH merger detected by a gravitational wave interferometer. We show how the very existence of the initial hollow can lead to super-Eddington accretion during this secular phase if the rate is not very far below Eddington prior to decoupling. Our model, though highly idealized, may be useful in establishing some of the key parameters, thermal emission features and scalings that characterize this transient. It can serve as a guide in the design and calibration of future radiation-magnetohydrodynamic simulations in general relativity.

## I. INTRODUCTION

Binary black holes (BHBHs) are among the most promising sources of gravitational waves detectable by gravitation-wave detectors such as LIGO [1, 2], VIRGO [3, 4], GEO [5], and TAMA [6, 7], as well as by the proposed space-based interferometers LISA [8], BBO [9] and DECIGO [10]. The development of stable algorithms to integrate Einstein’s field equations of general relativity numerically in 3+1 dimensions, such as the BSSN formalism [11, 12] and the generalized harmonic approach [13], together with the identification of suitable gauge conditions, enabled several pioneering simulations that demonstrated how to track the late inspiral, plunge and merger of a binary black hole (BHBH) in vacuum [14, 15, 16]. More refined follow-up simulations of these strong-field, late phases, joined onto to analytic, post-Newtonian calculations of the early inspiral epoch [17], are now capable of producing accurate gravitational waveforms for merging BHBH binaries with companions spanning a range of mass ratios and spins. These theoretical waveforms will be important as templates both for the detection of BHBH binaries and for the determination of their physical parameters, such as the masses and spins of the binary companions and the black hole remnant.

With the binary BHBH merger problem in vacuum well in hand, it is now important to turn to the problem of BHBH coalescence in astrophysically realistic gaseous environments in general relativity. When the orbit of the

BHBH binary is sufficiently close, the ambient gas should have little influence on the BHBH dynamics, but the impact of the black hole on the gas will be considerable. In particular, the capture, shock heating and accretion of gas may result in appreciable electromagnetic radiation. Such an “afterglow” could provide another observable signature of BHBH coalescence in addition to gravitational waves. Electromagnetic radiation can also serve as a useful probe of the gas in galaxy cores or in other environments where mergers may take place, as well as a probe of the physics of black hole accretion.

The effect of a BHBH system on a rotationally supported, geometrically thin, circumbinary disk has already triggered several important investigations, most in Newtonian gravitation. One key finding is that the Bardeen & Petterson mechanism [18] will align the disk to the orbital plane of the binary on a viscous timescale [19, 20]. Another result, first appreciated in the context of disks around pre-main-sequence binaries and protoplanets orbiting a central star, is that the disk is truncated at an inner edge  $r_{\text{edge}}$  where gravitational tidal torques arising from the binary and viscous stresses in the disk balance each other [21]. As a result, a hollowed-out region (“donut hole”) forms in the disk, causing gas accretion onto the black holes to remain well below the rate it would have in the absence of tidal torques. During the binary inspiral, viscosity in the disk keeps the ratio of the inner edge radius to the semimajor axis  $a$  of the binary roughly constant:  $r_{\text{edge}}/a \sim 1.5 - 2$  [21, 22, 23, 24]. Eventually, the binary separation shrinks sufficiently that the binary inspiral timescale due to gravitational wave emission becomes shorter than the viscous timescale in the disk. At this point, the binary “decouples” from the disk, and the inspiral proceeds all the way to plunge and merger while the disk barely evolves [25, 26, 27]. The

---

\*Also Department of Astronomy and NCSA, University of Illinois at Urbana-Champaign, Urbana, IL 61801

black hole remnant quickly settles down to a quasistationary state, after which the disk gas begins to drift inward on a secular, viscous timescale, filling the hollow down to the innermost stable circular orbit (ISCO) of the remnant black hole at  $r_{\text{isco}}$ . Eventually the disk settles down into quasistationary equilibrium and accretes at a steady rate onto the remnant. The scenario described here is summarized schematically in Fig. 1.

In this paper we follow the *secular* viscous evolution of a gaseous accretion disk following decoupling. We perform a simple, Newtonian calculation to determine the time-dependent inspiral and structure of a geometrically thin disk as it fills up the hollow region and flows into the black hole remnant. We also calculate the associated thermal radiation spectrum of the disk from the time of decoupling to the establishment of disk equilibrium. Our model is highly idealized in that we assume a radiation spectrum at each radius given by thermal black body emission at the local effective temperature. In a numerical example chosen to illustrate the model we also adopt a constant (turbulent) viscosity in space and time. While idealized and largely pedagogical, the model provides a reasonable first approximation to the relevant time and length scales characterizing such a scenario, as well as the typical magnitudes and frequencies of the associated accretion-driven electromagnetic afterglow. The model may be useful in designing and calibrating future, more detailed, simulations that employ more realistic microphysics and relativistic gravitation. Finally, adopting such a simple description for this transient yields a calculation that exhibits considerable scale freedom. In particular, the time-dependent solution to the nondimensional evolution equation that governs the gas inflow is uniquely determined by specifying only two free parameters in the initial data, the radius of the disk at decoupling,  $r_1$  and the BH remnant ISCO,  $r_{\text{isco}}$ . All other parameters may be scaled out of the problem. Moreover, given these two parameters, the equation does not depend on any further details of the disk microphysics.

Several recent calculations and hydrodynamic simulations have studied the *prompt* response of the circumbinary gas disk to gravitational wave-driven BHBH mass loss and remnant recoil following merger (see, e.g., [28, 29, 30, 31, 32] and references therein). The simulations treat effects that can occur on a hydrodynamical timescale in the absence of kinematic (shear) viscosity. They arise from those perturbations of the disk that are induced by the time-varying gravitational field of the binary just prior to merger and the recoiling remnant after merger. In fact, viscosity is typically ignored in these simulations. By contrast, the scenario considered below focusses on the slower, secular release of energy that ultimately accompanies the viscosity-driven inflow and accretion of the bound, rotating gas in the disk onto the remnant. The idealized model we adopt strictly applies only when the recoil speed of the central remnant is low, in which case the remnant remains near the center of the hollowed disk as it accretes. For nonspinning

black holes, the recoil speed is identically zero for equal-mass companions and small for companions of very unequal mass, falling roughly as  $q^2$ , where  $q < 1$  is the mass ratio. It reaches a maximum of about 175 km/s for  $q \approx 0.36$  (see [33] for a review and references). For spinning black holes of comparable mass the recoil can be much larger, but it is very sensitive to the spin magnitudes and orientations [34] and again decreases as  $q^2$ . Recoil speeds are estimated to be low ( $< 200$  km/s) in most galactic mergers [35]. Recent simulations of BHBHs orbiting inside circumnuclear disks in merged galaxy remnants give a median recoil speed that is quite low,  $< 70$  km/s [36]. Determining the distribution of pre-merger BHBH masses, mass ratios, spins and spin orientations remains an area of active investigation. We anticipate that in generic cases, both hydrodynamical (e.g shock) and secular (viscous) dissipation of energy are generated in the disk following decoupling and contribute to the radiation afterglow. We also anticipate that turbulent magnetic fields will provide the main source of (effective) viscosity in a realistic accretion disk. Future simulations will therefore need to incorporate magnetic fields to treat all phases of the afterglow properly.

We adopt geometrized units and set  $G = 1 = c$  below.

## II. BASIC MODEL

We focus on the epoch following the decoupling of the binary BHBH from the circumbinary accretion disk. Our calculation begins when the inner radius of the disk reaches the decoupling radius  $r_1$  and we follow its evolution as it fills in the hollow around the merged remnant,  $M$ . We adopt Newtonian physics throughout. We assume that just prior to decoupling the balance between tidal torques from the binary and viscous stresses in the disk results in a near-equilibrium disk which has the profile of a stationary thin disk with an “effective ISCO” at  $r_1$ . We take the outer boundary of the disk to be infinite. This constitutes our initial data.

As the gas loses angular momentum and diffuses inward from  $r_1$  following decoupling, we assume that it continues to inspiral in Keplerian circular orbits about the central black hole in the thin-disk approximation. We adopt axisymmetry about the rotation axis of the disk and neglect the self-gravity of gas in the disk. We take the inner boundary of the inspiraling disk to be the remnant black hole ISCO,  $r_{\text{isco}}$ , where we assume that viscous torques vanish.

In our model we assume that the energy dissipated by turbulent viscosity in the disk is all emitted as thermal black body radiation at the local effective temperature. Thus the net flux is a time-dependent superposition of local black body spectra from concentric annuli in the evolving disk, both inside and outside  $r_1$ . The *magnitude* of the integrated (total) radiated flux does not depend on the black body assumption and is independent of the detailed microphysics governing the (vertical) struc-

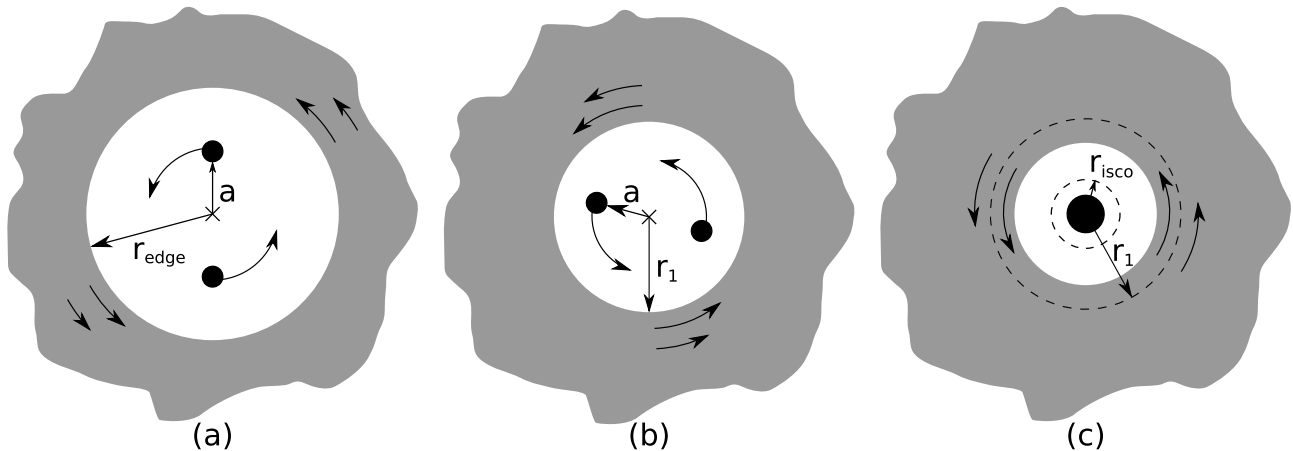


FIG. 1: Schematic figure of a Keplerian accretion disk orbiting a coalescing binary black hole. (a) The balance between tidal torques and viscosity maintains the inner edge of the disk at  $r_{\text{edge}} \sim 1.5a - 2a$ , where  $a$  is the binary semimajor axis. (b) Eventually the binary reaches a critical separation at which its inspiral timescale due to gravitational wave emission equals the viscous timescale in the disk. (c) The disk then decouples from the binary, which coalesces, leaving a central black hole remnant. Viscosity in the disk drives gas toward the remnant, filling up the hollow between the decoupling radius  $r_1$  and the ISCO radius  $r_{\text{isco}}$ .

ture of the disk, including its local scale height, viscosity, pressure, temperature, and opacity. In an illustrative example we set the turbulent viscosity  $\nu$  to be constant, noting that in some  $\alpha$ -disk models the viscosity is found to be a weak function of radius [27]. The magnitude of the viscosity, which does depend on the adopted microphysics, establishes the physical timescale for the inward diffusion of gas in the disk, but it can be scaled out of the numerical evolution of the disk and the emission. The disk microphysics is also important for determining standard “modifications” to the black body spectrum arising from, e.g., the dominance of electron scattering over true absorption in the inner region of the disk, as well as from comptonization or synchrotron radiation [37]. These effects tend to increase the color temperature above the effective temperature of the radiation and thereby harden the emitted spectrum. We postpone any consideration of these refinements to a future analysis.

### III. BASIC EQUATIONS

#### A. Disk Structure

The evolution equation for the surface density  $\Sigma(t, r)$  in an axisymmetric, geometrically-thin disk may be derived by combining the equation of mass conservation (continuity equation) and the equation of angular momentum conservation (the  $\phi$ -component of the Navier-Stokes equation). The result is [38]

$$\frac{\partial \Sigma}{\partial t} = \frac{3}{r} \frac{\partial}{\partial r} \left( r^{1/2} \frac{\partial}{\partial r} (\nu \Sigma r^{1/2}) \right), \quad (1)$$

where  $r$  is the cylindrical radius measured from the disk axis (or black hole remnant),  $t$  is the time and  $\nu$  is the

viscosity, which can be quite general at this point (i.e.,  $\nu = \nu(t, r)$ ). Equation (1) assumes that the angular velocity of the disk is Keplerian,  $\Omega = (M/r^3)^{1/2}$ . Taking the accretion rate at infinity to be independent of time, we seek to solve the equation subject to the following boundary conditions:

$$\text{b.c.'s: } \nu \Sigma = \begin{cases} (\nu \Sigma)_{\infty} = \text{constant}, & r \rightarrow \infty \\ 0, & r = r_{\text{isco}} \end{cases}. \quad (2)$$

For initial conditions, we shall take the system immediately after black hole merger at the center of the disk hollow. At merger the disk has not changed appreciably from its structure at decoupling, given that the viscous timescale is much longer than the BHBH inspiral timescale after decoupling. Prior to decoupling the balance between tidal torques and viscous stresses produces a near-equilibrium disk with an “effective ISCO” at  $r_1 = r_{\text{edge}} \sim 1.5a - 2a$ , where  $a$  is the semimajor axis of the binary. Consequently, we take the initial disk to be an equilibrium solution to equation (1) (i.e. a solution to  $\partial \Sigma / \partial t = 0$ ) satisfying the boundary conditions

$$t = 0: \quad \nu \Sigma = \begin{cases} (\nu \Sigma)_{\infty}, & r \rightarrow \infty \\ 0, & r = r_1 \end{cases}. \quad (3)$$

The initial profile of the disk is therefore a “donut” described by

$$t = 0: \quad \nu \Sigma = \begin{cases} (\nu \Sigma)_{\infty} \left( 1 - (r_1/r)^{1/2} \right), & r \geq r_1 \\ 0, & r < r_1 \end{cases}. \quad (4)$$

In fact, the profile of the final equilibrium disk, formed once the “donut” hole fills with gas down to  $r_{\text{isco}}$  and

settles down, has a similar, familiar form,

$$t = \infty : \quad \nu\Sigma = \begin{cases} (\nu\Sigma)_\infty \left(1 - (r_{\text{isco}}/r)^{1/2}\right), & r \geq r_{\text{isco}} \\ 0, & r < r_{\text{isco}} \end{cases}. \quad (5)$$

The goal is to solve equation (1) for the transient evolution during the interval  $0 < t < \infty$ .

The accretion rate  $\dot{M}(t, r) = 2\pi r \Sigma v_r$ , where  $v_r$  is the inward radial velocity of the gas, may be calculated from

$$\begin{aligned} \dot{M}(t, r) &= - \left[ \frac{\partial(r^2 \Omega)}{\partial r} \right]^{-1} \frac{\partial G}{\partial r}, \\ &= 6\pi r^{1/2} \frac{\partial(r^{1/2} \nu \Sigma)}{\partial r}. \end{aligned} \quad (6)$$

In equation (6) the quantity  $G(t, r)$  is the viscous torque [38],

$$G(t, r) = 2\pi r^3 \nu \Sigma \frac{\partial \Omega}{\partial r}, \quad (7)$$

evaluated for Keplerian motion. Using equation (2) to evaluate the accretion rate as  $r \rightarrow \infty$  yields

$$\dot{M}_\infty \equiv \dot{M}(t, \infty) = 3\pi(\nu\Sigma)_\infty = \text{constant}. \quad (8)$$

Equation (8) relates the asymptotic accretion rate to the asymptotic disk structure, both of which remain constant during the transient. This scenario is consistent with the notion that conditions far away from the central binary control the rate at which gas is fed into the disk.

To solve equation (1), which in general is nonlinear, it is convenient to introduce the following nondimensional variables:

$$\begin{aligned} s &= (r/r_1)^{1/2}, \quad \bar{\Sigma} = \Sigma/\Sigma_\infty, \quad y = s\bar{\Sigma}, \\ \bar{\nu} &= \nu/\nu_\infty, \quad \tau = t/t_{\text{vis}}, \end{aligned} \quad (9)$$

where

$$t_{\text{vis}} = \frac{4}{3} \frac{r_1^2}{\nu_\infty} \quad (10)$$

is a viscous timescale. In terms of these variables, equation (1) becomes

$$\frac{\partial y}{\partial \tau} = \frac{1}{s^2} \frac{\partial^2 (y\bar{\nu})}{\partial s^2}, \quad (11)$$

and must be integrated subject to boundary conditions

$$\text{b.c.'s:} \quad y = \begin{cases} s, & s \rightarrow \infty \\ 0, & s = (r_{\text{isco}}/r_1)^{1/2} \end{cases} \quad (12)$$

and initial conditions

$$t = 0 : \quad y = \begin{cases} (s-1)/\bar{\nu}, & s \geq 1 \\ 0, & s < 1 \end{cases}. \quad (13)$$

## B. Afterglow Radiation

The rate of viscous dissipation per unit surface area of the disk is given by [38]

$$D_{\text{vis}}(t, r) = \frac{9}{8} \nu \Sigma \frac{M}{r^3}. \quad (14)$$

Evolution equation (1) or (11) must be solved to determine the transient dissipation rate (14) as the disk fills up the hollow and then causes the region outside the original hollow to adjust in response. Assuming that this energy is all radiated locally, and approximating the emission to be a thermal blackbody radiation, the local disk surface temperature  $T_s(t, r)$  may be equated to the effective temperature, which is determined by the dissipation rate according to

$$\sigma T_s^4(t, r) = D(t, r) = \frac{9}{8} \nu \Sigma \frac{M}{r^3}, \quad 0 \leq t \leq \infty, \quad (15)$$

where  $\sigma$  is the Stefan-Boltzmann constant. For the initial and final equilibrium disks described by equations (4) and (5) the result can be found immediately:

$$\sigma T_s^4(t_{\text{eq}}, r) = \begin{cases} \left(3M\dot{M}_\infty/8\pi r^3\right) \left(1 - (r_{\text{eq}}/r)^{1/2}\right), & r \geq r_{\text{eq}} \\ 0, & r < r_{\text{eq}} \end{cases}, \quad (16)$$

where

$$t_{\text{eq}} = \begin{cases} 0, & r_{\text{eq}} = r_1, \\ \infty, & r_{\text{eq}} = r_{\text{isco}} \end{cases}. \quad (17)$$

For the transient, the temperature must be determined numerically by integrating equation (11) and substituting the result into equation (15).

Given the surface temperature, the transient specific flux  $F_\nu(t)$  measured by an observer at distance  $d$  whose line of sight makes an angle  $i$  to the normal to the disk plane is determined by integrating over the entire disk surface,

$$F_\nu(t) = \frac{2\pi \cos i}{d^2} \int_{r_{\text{isco}}}^{\infty} B_\nu(T_s(t', r)) r dr, \quad (18)$$

where  $B_\nu(T_s(t', r))$  is the Planck function,  $t' = t - d$  is retarded time and  $\nu$  is the photon frequency [39]. Equation (18) is best evaluated in terms of a nondimensional function  $f^*(t', x)$  of nondimensional frequency  $x$  according to

$$F_\nu(t) = \frac{2\pi \cos i}{d^2} \frac{15}{\pi^5} \frac{\sigma T_*^4}{\nu_*^2} r_{\text{isco}}^2 f^*(t', x), \quad (19)$$

where

$$f^*(t', x) \equiv \int_1^\infty du \, u \frac{x^3}{\exp(xT_*/T_s) - 1}, \quad (20)$$

and where we have introduced the parameters

$$\sigma T_*^4 \equiv 3M\dot{M}_\infty/8\pi r_{\text{isco}}^3, \quad h\nu_* \equiv kT_*,$$

$$x \equiv h\nu/kT_* = \nu/\nu_*, \quad u \equiv r/r_{\text{isco}}. \quad (21)$$

The quantity  $T_*$  provides an estimate of the characteristic temperature in the main radiating region of the final equilibrium disk, which resides near  $r_{\text{isco}}$ , and  $h\nu_*$  is the characteristic frequency of the emitted thermal radiation from this region. The specific luminosity  $L_\nu(t)$ , summing over both surfaces of the disk, is related to  $F_\nu(t)$  according to

$$L_\nu(t) = \frac{2\pi d^2}{\cos i} F_\nu(t). \quad (22)$$

The total luminosity  $L(t)$  integrated over all frequencies is then given by

$$L(t) = \int_0^\infty d\nu L_\nu(t) = \frac{60}{\pi^3} \sigma T_*^4 r_{\text{isco}}^2 \int_0^\infty f^*(t', x) dx \quad (23)$$

The the initial and final equilibrium disks provide analytic temperature profiles (i.e. equation 16), from which the fluxes can be determined without knowing the transient evolution. At low frequencies  $x \ll (r_{\text{isco}}/r_{\text{eq}})^{3/4}$ , where  $r_{\text{eq}}$  is defined in equation (17), we have

$$f^*(t_{\text{eq}}, x) \approx \frac{4}{3} \Gamma(8/3) \zeta(8/3) x^{1/3}, \quad (24)$$

where  $\Gamma(8/3) = 1.50457$  and  $\zeta(8/3) = 1.28419$ . To derive this result we have used the approximation  $T_*/T_s(t_{\text{eq},r}) \approx (r/r_{\text{isco}})^{3/4}$  in the outer disk where the low-frequency radiation is generated, together with the identity

$$\Gamma(s) \zeta(s) = \int_0^\infty \frac{x^{s-1}}{\exp(x) - 1} dx. \quad (25)$$

Equations (19) and (24) combine to give the well-known low-frequency component of the thin-disk thermal spectrum,  $F_\nu \sim \nu^{1/3}$ . The total integrated luminosity and flux from the initial and final disk also can be obtained analytically. Using the identity

$$\int_0^\infty f^*(t'_{\text{eq}}, x) dx = \frac{\pi^4}{45} \frac{r_{\text{isco}}}{r_{\text{eq}}} \quad (26)$$

in equation (23) gives

$$L(t_{\text{eq}}) = \frac{4}{3} \pi \sigma T_*^4 r_{\text{isco}}^2 \frac{r_{\text{isco}}}{r_{\text{eq}}} \quad (27)$$

or, equivalently,

$$L(t_{\text{eq}}) = \begin{cases} M\dot{M}_\infty/2r_1, & t'_{\text{eq}} = 0, \\ M\dot{M}_\infty/2r_{\text{isco}}, & t'_{\text{eq}} = \infty \end{cases}. \quad (28)$$

Equation (28) recovers the standard result for the total luminosity of a thin accretion disk with an inner boundary at  $r_{\text{eq}}$ . This result is customarily obtained directly from the integral

$$L(t) = 2 \int_{r_{\text{eq}}}^\infty \sigma T_s^4 2\pi r dr = 2 \int_{r_{\text{eq}}}^\infty \frac{9}{8} (\nu\Sigma) \frac{M}{r^3} 2\pi r dr, \quad (29)$$

substituting equations (4) and (5) for the two equilibrium profiles. Its significance for afterglow radiation is that, at least in our simple model, the total electromagnetic flux will increase from its value immediately after BHBH merger (as signaled by peak gravitational wave emission) to a value that is larger by a factor of  $r_1/r_{\text{isco}}$  as the disk settles into final equilibrium. The timescale over which the increase will occur will be the viscous timescale near the decoupling radius in the disk,  $r_1$ . In the next section we calculate the time-varying evolution and electromagnetic emission during this transition.

## IV. THE TRANSIENT AFTERGLOW: AN ILLUSTRATIVE EXAMPLE

### A. Nondimensional Description

Equation (11) is a parabolic, nonlinear, diffusion equation with a variable diffusion coefficient (e.g., the coefficient decreases as  $s^{-2}$  for the linear case with constant  $\bar{\nu}$ ). In general, such a nonlinear equation must be integrated numerically, which, in anticipation of future applications, motivates our approach here. However, there are standard analytic (e.g. Green function) techniques that can be implemented for the linear case [38]. We adopt a Crank-Nicholson finite-difference scheme, which is fully implicit and second order in both space and time. Such an implicit scheme is well-suited to accommodate the large spatial extent of the disk that must be covered to implement the boundary conditions. This coverage is facilitated by introducing a logarithmic grid in  $s$  from  $s = (r_{\text{isco}}/r_1)^{1/2} \ll 1$  to  $s \gg 1$  [40]. Since a Crank-Nicholson scheme is unconditionally stable for numerical timesteps of arbitrary size, the step size is restricted only by accuracy considerations and not grid spacing and can be much larger than that required by the usual Courant condition for explicit schemes.

To illustrate the transient behavior with a simple model, we take the viscosity in the disk to be a constant, in which case  $\bar{\nu} = 1$ . Equation (11) is then uniquely determined by setting  $r_{\text{isco}}$  and  $r_1$ . We set  $r_{\text{isco}} = 6M$ , the value appropriate for a Schwarzschild black hole remnant [41], and  $r_1 = 100M$ , a choice consistent with some recent estimates of disk properties at binary BHBH-disk decoupling [42].

The growth of the surface density  $\Sigma(t, r)$  inside and outside the hollow following decoupling and merger is shown in Fig. 2. The associated growth in the local accretion rate  $\dot{M}(t, r)$  (see equation 6) is plotted in Fig. 3. The secular transition from the initial to final equilibrium disk is evident as gas migrates inward toward the black hole remnant.

The transient thermal spectrum (equations 19 and 20) is plotted in Fig. 4. The spectrum hardens and the total flux and luminosity increase in magnitude as the hollow fills with (radiating) matter. In analogy to equation (21),

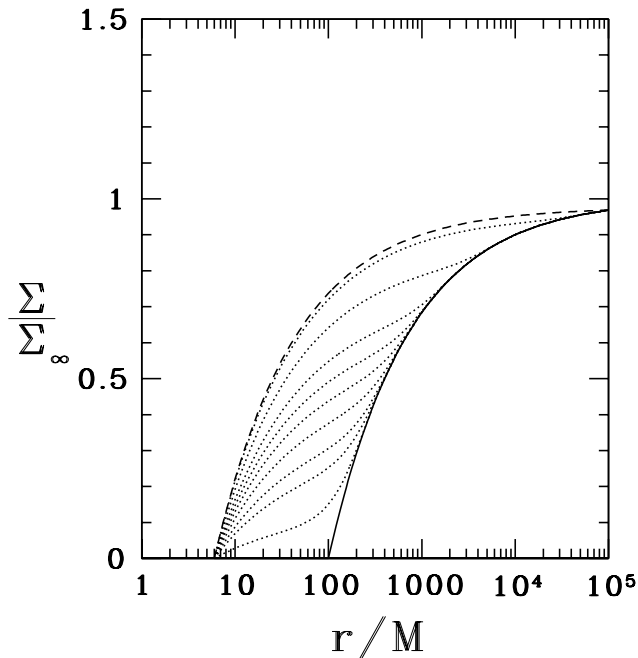


FIG. 2: Profiles of the disk surface density  $\Sigma$  at select times  $\tau$  during accretion following the binary BHBH merger. The disk decoupling radius is at  $r_1 = 100M$  and the ISCO is at  $r_{\text{isco}} = 6M$ , where  $M$  is the mass of the black hole remnant. The initial (final) equilibrium disk is indicated by the heavy solid (dashed) curve. Profiles at intermediate times are shown by dotted curves at  $\tau = 0.0694, 0.208, 0.347, 0.694, 1.39, 2.78, 6.94, 69.4$  and  $6940$ .

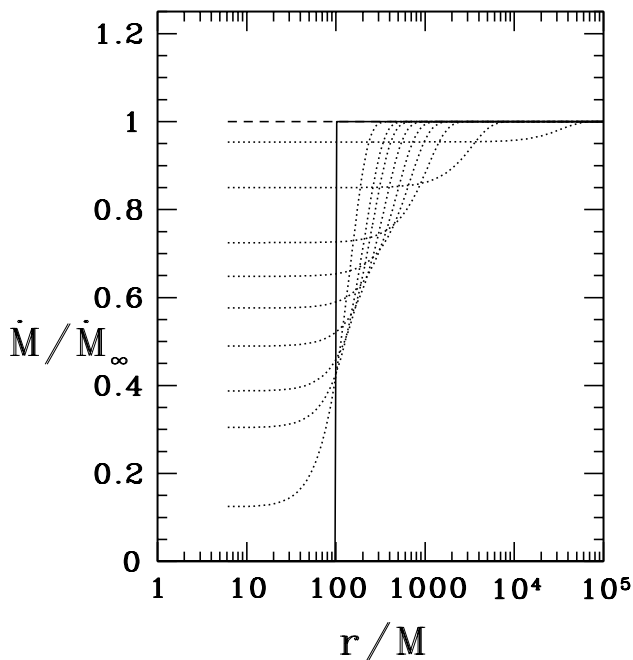


FIG. 3: Profiles of the local disk accretion rate  $\dot{M}$  at select times  $\tau$  following the binary BHBH merger (see equation 6). The curves are labeled as in Fig. 2.

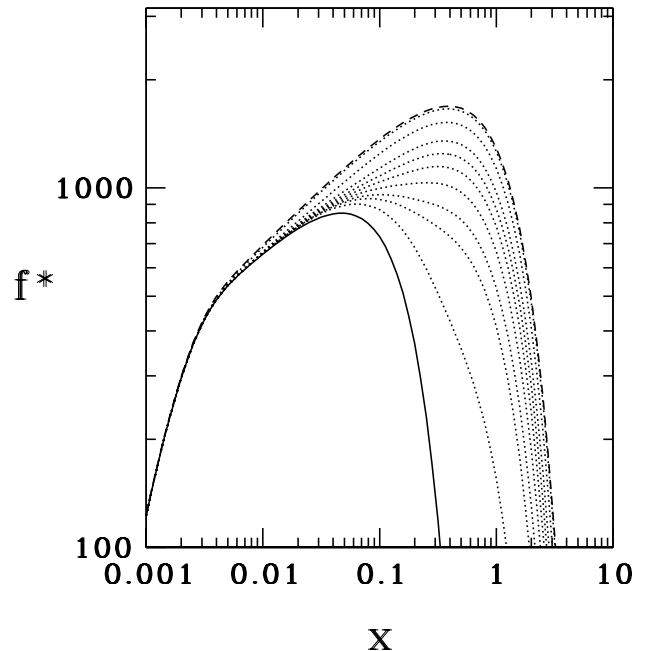


FIG. 4: The frequency distribution of the emitted electromagnetic thermal radiation at select times  $\tau$  following the binary BHBH merger. The nondimensional distribution function  $f^*$  and photon frequency  $x$  are defined in equations (19)–(21). The curves are labeled as in Fig. 2.

define the quantities

$$\sigma T_1^4 \equiv 3M\dot{M}_\infty/8\pi r_1^3, \quad h\nu_1 \equiv kT_1 \quad (30)$$

which characterize conditions near the inner edge of the initial disk. The peak frequency evolves from near  $\nu_1$  to  $\nu_*$  over the course of the transient, where  $\nu_*/\nu_1 = (r_1/r_{\text{isco}})^{3/4} \approx 8.2$  in our example. Over the same time frame, the total luminosity increases according to equation (28), whereby  $L(\infty)/L(0) = r_1/r_{\text{isco}} \approx 16.7$  in this example [43].

The increase in total luminosity is plotted as a function of time in Fig. 5. The characteristic timescale over which the transient lasts is  $\delta\tau \sim 10 - 100$ , or, according to equations (9) and (10),  $\delta t \sim (10 - 100) t_{\text{vis}}$ . We note that the timescale  $t_{\text{vis}}$  defined by equation (9) is related to the viscous timescale at the inner edge of initial disk,  $r_1$ , where the initial surface density,  $\Sigma(0, r_1)$ , is identically zero (equation 4). The gas that establishes the final equilibrium flow at the ISCO originates from radii  $r \gg r_1$ , where the density  $\Sigma(0, r)$  is nonzero and closer to its final equilibrium value. Since the viscous timescale on which this gas drifts inward varies like  $r^2$ , the equilibration timescale is therefore much longer than  $t_{\text{vis}}$ .

The luminosity increase with time is directly correlated with the increase in the accretion rate at the ISCO, as is evident from Fig. 5. That the two curves plotted in the figure line up so closely once the transient gets underway

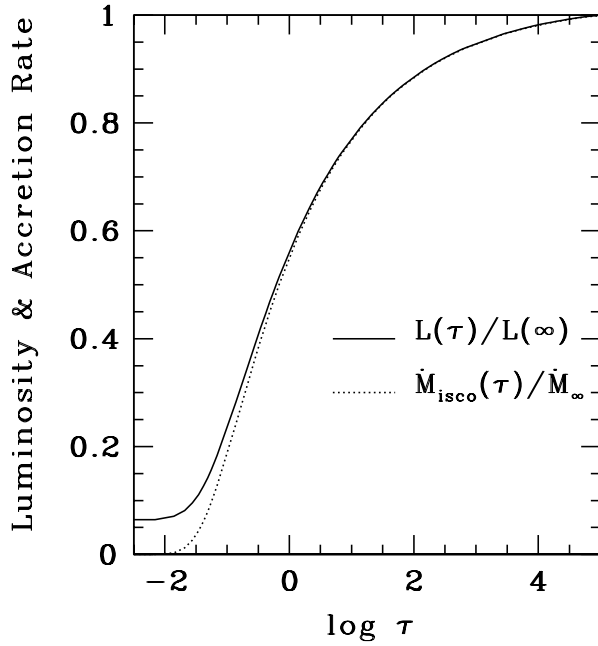


FIG. 5: The increase in luminosity  $L$  and ISCO accretion rate  $\dot{M}_{\text{isco}}$  with time  $\tau$  during accretion following the binary BHBH merger. Note that the time coordinate for  $\dot{M}_{\text{isco}}$  represents retarded time.

( $\tau \gtrsim 0.1$ ) can be explained as follows: during this epoch, the surface density in the main radiating, inner region is found numerically to satisfy the approximate relation

$$\nu\Sigma(t, r) \approx C(t) \left(1 - (r_{\text{isco}}/r)^{1/2}\right), \quad (31)$$

where the factor  $C(t)$  climbs from near zero initially to its late, asymptotic value  $C(\infty) = (\nu\Sigma)_{\infty}$  (see equation 5). Using equation (31) in equation (29) yields

$$L(t)/L(\infty) \approx C(t)/(\nu\Sigma)_{\infty}. \quad (32)$$

Using equation (31) in equation (6) to calculate  $\dot{M}_{\text{isco}}(t)$ , and inserting equation (8), then gives

$$\dot{M}_{\text{isco}}(t)/\dot{M}_{\infty} \approx L(t)/L(\infty), \quad (33)$$

which explains the numerical result revealed in Fig. 5. Consistent with the fit (31) for the surface density is the implication that the accretion rate in innermost region near the ISCO must be nearly independent of  $r$  during the transient,  $\dot{M}(t, r) \approx 3\pi C(t)$ . This result is verified numerically in Fig. 3.

## B. Physical Units and Scaling

To be astrophysically useful and applicable to general cases we need to restore physical units to our nondimensional numerical solution and provide appropriate scaling with the independent physical parameters. Toward

this end we define several auxiliary quantities, including the black hole mass parameter  $M_6 = M/10^6 M_{\odot}$ , the distance parameter  $d_{10} = d/10$  Mpc, and the accretion rate in Eddington units,  $\dot{m}_E = \dot{M}/\dot{M}_E$ , where  $\dot{M}_E = 12L_E/c^2 = 1.68 \times 10^{24} M_6$  gm/s is the Eddington accretion rate for the final equilibrium disk [44] and  $L_E = 1.26 \times 10^{44} M_6$  erg/s is the Eddington luminosity. In terms of these parameters, we have

$$\begin{aligned} T_* &= 0.906 \times 10^6 \dot{m}_E^{1/4} M_6^{-1/4} \text{ K}, \\ \nu_* &= 1.89 \times 10^{16} \dot{m}_E^{1/4} M_6^{-1/4} \text{ Hz}, \\ &= 78.1 \dot{m}_E^{1/4} M_6^{-1/4} \text{ eV/h}, \\ \frac{\sigma T_*^4 r_{\text{isco}}^2}{\nu_* d^2} &= 1.67 \times 10^{-24} \dot{m}_E^{3/4} M_6^{5/4} d_{10}^{-2} \frac{\text{erg}}{\text{cm}^2 \text{ s Hz}}, \\ L(\infty) &= 1.26 \times 10^{44} \dot{m}_E \text{ erg/s}. \end{aligned} \quad (34)$$

The above quantities set the scale for the characteristic innermost disk temperature, peak thermal photon frequency, observed thermal flux and total thermal luminosity for the final equilibrium disk with  $r_{\text{isco}} = 6M$ . The fourth line provides the scale factor that appears in equation (19) for the specific flux. Using this factor together with Fig. 4 yields the transient spectrum in physical units.

The corresponding parameters for the initial disk at decoupling, with  $r_1 = 100M$ , are given by

$$\begin{aligned} T_1 &= 0.653 \times 10^5 \dot{m}_E^{1/4} M_6^{-1/4} \text{ K}, \\ \nu_1 &= 1.36 \times 10^{15} \dot{m}_E^{1/4} M_6^{-1/4} \text{ Hz}, \\ &= 5.63 \dot{m}_E^{1/4} M_6^{-1/4} \text{ eV/h}, \\ \frac{\sigma T_1^4 r_1^2}{\nu_1 d^2} &= 0.695 \times 10^{-24} \dot{m}_E^{3/4} M_6^{5/4} d_{10}^{-2} \frac{\text{erg}}{\text{cm}^2 \text{ s Hz}}, \\ L(0) &= 0.754 \times 10^{43} \dot{m}_E \text{ erg/s}. \end{aligned} \quad (35)$$

The fact that the thermal emission hardens and increases in magnitude during the transient is again evident by comparing equations (34) and (35). For black holes of mass  $M_6 \approx 1$  accreting at  $\dot{m}_E \approx 0.1$  the peak emission at the start of the transient lies in the *UV* band and then hardens to *EUV* and soft *X-ray* radiation at late times [45].

None of the physical disk structure or emission frequencies and magnitudes calculated above depend on any details of the disk microphysics in our idealized model. However, we do need to probe the microphysics in order to assign a physical *timescale* to the transient. The dimensional time parameter  $\tau$  can be translated into physical time only when  $t_{\text{vis}}$  appearing in equation (10) has been evaluated, and for that we need to know the viscosity. Our numerical implementation assumed a constant viscosity in the disk. To get a realistic estimate of the appropriate value to use we can adopt the standard Shakura and Sunyaev [46]  $\alpha$ -disk model and employ the value it gives for the turbulent viscosity at  $r_1$ . In this model, the radius  $r_1$  will reside in the “inner region”, where the pressure is radiation-dominated and the opacity is electron scattering-dominated, provided it lies within a

critical radius  $r_{\text{in}}$ , where [47, 48]

$$r_{\text{in}}/M \approx 2.56 \times 10^3 \alpha^{2/21} \dot{m}_E^{16/21} M_6^{2/21}. \quad (36)$$

For those cases in which  $r_1 < r_{\text{in}}$  [27] the viscous timescale at  $r_1/M = 100$  is

$$t_{\text{vis}} \approx 2.54 \times 10^5 \alpha^{-1} \dot{m}_E^{-2} M_6 \text{ sec}. \quad (37)$$

Hence for the case  $M_6 = 1$ ,  $\dot{m}_E = 0.1$  and  $\alpha = 0.1$  we obtain  $t_{\text{vis}} = 8.1$  yr. For other cases,  $r_1$  may lie in the gas-pressure dominated region and the estimate for  $t_{\text{vis}}$  will be quite different [29].

In reality, secular gas inflow in the hollow following BHBH merger is likely controlled by magnetic fields that are driven turbulent by MRI and other instabilities [49]. The magnetic field thereby acts like an effective turbulent viscosity, but such a viscosity might exhibit very different scaling behavior from the standard  $\alpha$ -disk model. This issue, which is the subject of considerable interest and current research in the case of stationary disk accretion onto black holes, is clearly relevant in the case of transient, post-merger BHBH accretion, but it is beyond the scope of this paper and we shall not pursue it further.

### C. Super-Eddington Accretion?

The evolution calculated above assumes that the rate at which gas enters the disk is determined by conditions at large distance from the remnant black hole and remains constant in time during the transient. In cases for which the ambient gas densities are sufficiently low the merging BHBH may be ‘gas-starved’ and the accretion rate will be safely sub-Eddington during the entire evolution. However, an interesting scenario arises if there is sufficient gas in the neighborhood of the merging (‘gas-rich’) BHBH for the luminosity to exceed the critical Eddington limit  $L_E$ . Suppose, for example, that already by the time of merger the accretion rate  $\dot{m}(0)$

at  $r_1$  in the initial hollowed-out disk is sufficiently high to drive the luminosity  $L(0)$  to the critical Eddington value  $L_E$ . Then accretion at this same rate would cause the luminosity to exceed  $L_E$  during the subsequent transient phase, as the total disk luminosity steadily increases (see Fig. 5). According to equation (28) this initial accretion rate will be larger than the critical Eddington rate in the final equilibrium disk by a substantial factor:  $\dot{m}(\infty) = \dot{m}(0) = (r_1/r_{\text{isco}})\dot{m}_E > \dot{m}_E$ . Ignore for the moment the possibility that the geometrically thin-disk approximation could break down as  $L$  approaches  $L_E$  [50]. Since the viscous timescale increases rapidly with  $r$  (see, e.g., equation 10) the outer disk has insufficient time to adjust quasistatically and reduce the inflow rate to maintain  $L(t)$  at  $L_E$  as gas fills the hollow. What happens instead is unclear and may be complicated and highly dynamical. One possibility is that the disk puffs up, the accretion becomes almost spherical as the gas fills the hollow, and the local radiation pressure blows excess matter away to maintain  $L \approx L_E$ . Alternatively, density inhomogeneities resulting from the photon-bubble instability [51, 52] might keep the disk geometrically thin and allow radiation to escape through porous regions of very low density. In the latter case the escaping luminosity could exceed  $L_E$  by a considerable factor (10 – 100), accompanied by radiation-driven mass loss [53]. A full understanding of this super-Eddington scenario may require global, general relativistic, radiation-MHD simulations in 3 + 1 dimensions. Such a treatment may well be worthwhile, since this transition from quiescent sub-Eddington accretion to highly dynamical super-Eddington flow may provide another observable signature of binary BHBH mergers in ‘gas-rich’ regions.

*Acknowledgments:* It is a pleasure to thank C. Gamie and Y.T. Liu for useful discussions and D. Kotan for technical assistance. This paper was supported in part by NSF Grant PHY06-50377 and NASA Grant NNX07AG96G to the University of Illinois at Urbana-Champaign.

- 
- [1] B. Abbott and the LIGO Scientific Collaboration, Phys. Rev. D **77**, 062002 (2008).
  - [2] D. A. Brown, S. Babak, P. R. Brady, N. Christensen, T. Cokelaer, J. D. E. Creighton, S. Fairhurst, G. Gonzalez, E. Messaritaki, B. S. Sathyaprakash, et al., Class. Quant. Grav. **21**, S1625 (2004).
  - [3] F. Acernese and the VIRGO Collaboration, Class. Quant. Grav. **23**, 635 (2006).
  - [4] F. Beauville and the LIGO-VIRGO Working Group, Class. Quant. Grav. **25**, 045001 (2008).
  - [5] H. Lück and the GEO600 collaboration, Class. Quant. Grav. **23**, S71 (2006).
  - [6] M. Ando and the TAMA collaboration, Class. Quant. Grav. **19**, 1409 (2002).
  - [7] D. Tatsumi and the TAMA collaboration, Class. Quant. Grav. **24**, 399 (2007).
  - [8] G. Heinzl, C. Braxmaier, K. Danzmann, P. Gath, J. Hough, O. Jennrich, U. Johann, A. Rüdiger, M. Salusti, and H. Schulte, Class. Quant. Grav. **23**, 119 (2006).
  - [9] E. Phinney et al, NASA Mission Concept Study (2003).
  - [10] S. Kawamura and the DECIGO collaboration, Class. Quant. Grav. **23**, 125 (2006).
  - [11] M. Shibata and T. Nakamura, Phys. Rev. D **52**, 5428 (1995).
  - [12] T. W. Baumgarte and S. L. Shapiro, Phys. Rev. D **59**, 024007 (1999).
  - [13] F. Pretorius, Class. Quant. Grav. **22**, 425 (2005).
  - [14] F. Pretorius, Physical Review Letters **95**, 121101 (2005).
  - [15] M. Campanelli, C. O. Lousto, P. Marronetti, and Y. Zlochower, Physical Review Letters **96**, 111101 (2006).
  - [16] J. G. Baker, J. Centrella, D.-I. Choi, M. Koppitz, and J. van Meter, Physical Review Letters **96**, 111102 (2006).



- [17] L. Blanchet, G. Faye, B. R. Iyer, and S. Sinha, *Class. Quant. Grav.* **25**, 165003 (2008).
- [18] J. M. Bardeen and J. A. Petterson, *Astrophys. J. Lett.* **195**, L65 (1975).
- [19] J. D. Larwood and J. C. B. Papaloizou, *Mon. Not. R. Astro. Soc.* **285**, 288 (1997).
- [20] P. B. Ivanov, J. C. B. Papaloizou, and A. G. Polnarev, *Mon. Not. R. Astro. Soc.* **307**, 79 (1999).
- [21] P. Artymowicz and S. H. Lubow, *Astrophys. J.* **421**, 651 (1994).
- [22] R. Günther and W. Kley, *A&A* **387**, 550 (2002).
- [23] A. Escala, R. B. Larson, P. S. Coppi, and D. Mardones, *Astrophys. J.* **630**, 152 (2005).
- [24] A. I. MacFadyen and M. Milosavljević, *Astrophys. J.* **672**, 83 (2008).
- [25] P. J. Armitage and P. Natarajan, *Astrophys. J. Lett.* **567**, L9 (2002).
- [26] F. K. Liu, X.-B. Wu, and S. L. Cao, *Mon. Not. R. Astro. Soc.* **340**, 411 (2003).
- [27] M. Milosavljević and E. S. Phinney, *Astrophys. J. Lett.* **622**, L93 (2005).
- [28] S. M. O’Neill, M. C. Miller, T. Bogdanović, C. S. Reynolds, and J. D. Schnittman, *Astrophys. J.* **700**, 859 (2009).
- [29] J. D. Schnittman and J. H. Krolik, *Astrophys. J.* **684**, 835 (2008).
- [30] L. R. Corrales, Z. Haiman, and A. MacFadyen, *ArXiv e-prints* (2009), 0910.0014.
- [31] E. M. Rossi, G. Lodato, P. J. Armitage, J. E. Pringle, and A. R. King, *ArXiv e-prints* (2009), 0910.0002.
- [32] M. Anderson, L. Lehner, M. Megevand, and D. Neilsen, *ArXiv e-prints* (2009), 0910.4969.
- [33] T. W. Baumgarte and S. L. Shapiro, *Numerical relativity: Solving Einstein’s equations on the computer* (Cambridge University Press, Cambridge, in press, 2010).
- [34] For equal-mass companions with spins in the orbital plane and anti-aligned, the maximum recoil is about 4000 km/s; M. Campanelli, C. O. Lousto, Y. Zlochower, and D. Merritt, *Physical Review Letters* **98**, 231102 (2007).
- [35] T. Bogdanović, C. S. Reynolds, and M. C. Miller, *Astrophys. J. Lett.* **661**, L147 (2007).
- [36] M. Dotti, M. Volonteri, A. Perego, M. Colpi, M. Ruzsowski, and F. Haardt, *ArXiv e-prints* (2009), 0910.5729.
- [37] Details involving the disk microphysics are also required to estimate the fraction of the dissipated energy that may be advected rather than radiated; we neglect advection here.
- [38] J. E. Pringle, *A&A* **19**, 137 (1981).
- [39] From the context it should not be difficult to distinguish the photon frequency  $\nu$  from the viscosity  $\nu$ .
- [40] While the disk is presumed to be infinite, in practice we set its outer boundary at  $r = 10^5 M$  in our numerical integrations; the results are insensitive to the specific choice of outer radius for values this far out in the disk.
- [41] However, the remnant of two equal-mass, nonspinning BHBHs will be a rotating Kerr black hole with dimensionless spin parameter  $J^2/M \approx 0.688$ , for which  $r_{\text{isco}}/M \approx 3.45$  in Boyer-Lindquist coordinates; see, e.g., [33].
- [42] See, e.g., [27], who find that fiducial disk parameters give a decoupling binary separation  $a \approx 100M$ , scaling slowly with mass as  $(M/10^6 M_\odot)^{0.08} (4q/(1+q)^2)^{0.42}$ . See also [29], who find higher values of  $a$ .
- [43] Here our notation  $L(0)$  and  $L(\infty)$  refers to the initial and final equilibrium disks, respectively.
- [44] See equation (28), which is for a Newtonian disk and gives an accretion efficiency  $\eta = 1/12$  for  $r_{\text{isco}} = 6M$ .
- [45] Accounting for the dominance of electron scattering over free-free absorption opacity leads to a higher surface temperature by the well-known ratio  $(\kappa_{\text{es}}/\kappa_{\text{ff}})^{1/8} \sim \text{few}$ , and this, in turn, results in a higher thermal photon energy [27, 46, 47, 48].
- [46] N. I. Shakura and R. A. Sunyaev, *A&A* **24**, 337 (1973).
- [47] I. D. Novikov and K. S. Thorne, in *Black Holes, Les Houches*, edited by C. Dewitt and B. DeWitt (Gordon and Breach, New York, 1973), pp. 343–450.
- [48] S. L. Shapiro and S. A. Teukolsky, *Black holes, white dwarfs, and neutron stars: The physics of compact objects* (John Wiley, New York, 1983).
- [49] V.P. Velikhov, *Sov. Phys. JETP* **36**, 995 (1959); S. Chandrasekhar, *Proc. Natl. Acad. Sci. U.S.A.* **46**, 253 (1960); S.A. Balbus and J. F. Hawley, *Astrophys. J.* **376**, 214 (1991); *Rev. Mod. Phys.* **70**, 1 (1998).
- [50] J. Frank, A. King, and D. J. Raine, *Accretion power in astrophysics* (Cambridge University Press, Cambridge, 2002).
- [51] J. Arons, *Astrophys. J.* **388**, 561 (1992).
- [52] C. F. Gammie, *Mon. Not. R. Astro. Soc.* **297**, 929 (1998).
- [53] M. C. Begelman, *Astrophys. J. Lett.* **568**, L97 (2002).